1. AGENCY USE ONLY (Leave blank)	2. REPORT DATE	3. REPORT TYPE AND DATES COVERED
	August 1993	final report Jan 1 1992 - June 30 1993

4. TITLE AND SUBTITLE

Refractive Index Structure in the Lower Atmosphere

5. FUNDING NUMBERS

DAAL03-92-G-0004

6. AUTHOR(S)

J Wyngaard
D Thomson

7. PERFORMING ORGANIZATION NAME(S) AND ADDRESS(ES)

Department of Meteorology
The Pennsylvania State University
503 Walker Bldg
University Park PA 16802

8. PERFORMING ORGANIZATION REPORT NUMBER

9. SPONSORING / MONITORING AGENCY NAME(S) AND ADDRESS(ES)

U. S. Army Research Office
P. O. Box 12211
Research Triangle Park, NC 27709-2211

10. SPONSORING / MONITORING AGENCY REPORT NUMBER

ARO 29196.1-GS

11. SUPPLEMENTARY NOTES

The view, opinions and/or findings contained in this report are those of the author(s) and should not be construed as an official Department of the Army position, policy, or decision, unless so designated by other documentation.

12a. DISTRIBUTION / AVAILABILITY STATEMENT

Approved for public release; distribution unlimited.

12b. DISTRIBUTION CODE

13. ABSTRACT *(Maximum 200 words)*

We develop a local scaling theory for structure-function parameters C_N^2 and C_v^2 of refractive index and velocity fluctuations in the stably stratified atmospheric boundary layer. The theory relates them to the local values of vertical temperature flux $\overline{w\theta}$ and shearing stress τ. The theory agrees well with data from observations and from large-eddy simulations. The effects of flow unsteadiness, baroclinity, terrain slope, and breaking gravity waves are apt to cause the vertical profiles of $\overline{w\theta}$ and τ to vary strongly from case to case, making the C_N^2 and C_v^2 profiles quite variable as well, but according to the theory the stress and heat flux profiles can generally be diagnosed from those of the structure parameters.

14. SUBJECT TERMS

refractive index, structure-function parameters, turbulence, stable boundary layer, large-eddy simulation

15. NUMBER OF PAGES

33

16. PRICE CODE

17. SECURITY CLASSIFICATION OF REPORT	18. SECURITY CLASSIFICATION	19. SECURITY CLASSIFICATION OF ABSTRACT	20. LIMITATION OF ABSTRACT
UNCLASSIFIED	UNCLASSIFIED	UNCLASSIFIED	UL

REFRACTIVE INDEX STRUCTURE IN THE LOWER ATMOSPHERE

Final Report

J. Wyngaard, D. Thomson
August, 1993

U. S. Army Research Office
Grant Number DAAL03-92-G-0004

The Pennsylvania State University
Department of Meteorology
University Park, PA

Table of Contents

A. Statement of Problem Studied

Theoretical treatment of the scattering of electromagnetic and acoustic radiation usually focuses on the refractive index structure function (Tatarskii, 1971) which is defined by

$$\overline{[n(\mathbf{x},t)-n(\mathbf{x}+\mathbf{r},t)]^2} \equiv \overline{(n-n')^2}, \tag{1}$$

where n is the fluctuating refractive index at point $\mathbf{x}$ and n' that at point $\mathbf{x}+\mathbf{r}$. The overbar denotes the expected value (ensemble average). Many wave-propagation problems involve this structure function only for separations $r = |\mathbf{r}|$ in the inertial range of scales, where it has the form

$$\overline{(n-n')^2} = C_N^2 r^{2/3}. \tag{2}$$

We call C_N^2 the refractive index *structure-function parameter.*

Fluctuations in the refractive index for microwave radiation are caused primarily by fluctuations in temperature and absolute humidity, θ and q, respectively. One can write

$$n = a\theta + bq, \tag{3}$$

where the coefficients a and b depend on the wavelength of the radiation. Wyngaard et al. (1978) have shown that this implies that C_N^2 may be expressed in terms of the structure-function parameters for temperature and humidity, C_T^2 and C_Q^2, and the joint structure parameter, C_{TQ}:

$$C_N^2 = a^2 C_T^2 + 2abC_{TQ} + b^2 C_Q^2. \tag{4}$$

For acoustic radiation, the refractive index structure-function parameter depends additionally on C_v^2, the structure-function parameter for the velocity field.

The purpose of our research was to illuminate the physics of the maintenance of these structure-function parameters in the lower atmosphere and, in particular, to develop a theory for their vertical profiles in the stably stratified boundary layer.

B. Summary of Most Important Results

1. Local-scaling theory for structure-function parameters

Using a combination of observational and large-eddy-simulation data, we developed and tested a similarity theory for C_T^2 and C_v^2 in the stably stratified boundary layer. This theory relates these structure-function parameters to the vertical temperature flux and the shearing stress, basic structural variables in the stable boundary layer. Our theory uses the "local scaling" hypothesis for stably stratified shear flows. In this hypothesis the length, velocity, and temperature scales for the turbulence are taken as

$$\Lambda = -\frac{\tau^{3/2}T}{kg\overline{w\theta}}; \quad u_* = \tau^{1/2}; \quad T_* = \frac{-\overline{w\theta}}{u_*}, \tag{5}$$

where $\tau(z)$ and $\overline{w\theta}(z)$ are the local values of kinematic stress and temperature flux, respectively. The basic hypothesis is that dependent variables made dimensionless with these scales are universal functions of z/Λ. In effect, this generalizes Monin-Obukhov similarity to the entire stable boundary layer by replacing the the Monin-Obukhov length scale L with Λ.

The local scaling hypothesis has roots both in the behavior observed in the 1968 Kansas surface-layer experiments and other field programs (Wyngaard, 1973) as well as in Nieuwstadt's (1984) studies of a set of second-moment equations for the stable boundary layer. The Kansas data for wind and temperature gradients, velocity and temperature variances, and dissipation rates at large z/L (i.e., under very stable conditions in the surface layer) are consistent with local scaling. Nieuwstadt found that velocity and temperature statistics from the 200-m tower at Cabauw were also in good agreement with local-scaling predictions.

The local-scaling prediction for C_T^2 is

$$\frac{C_T^2 \Lambda^{2/3}}{T_*^2} = f(\frac{z}{\Lambda}), \tag{6}$$

where f is a universal function to be determined. In the very stable surface layer the Kansas data yield the M-O asymptote

$$\frac{C_T^2 L^{2/3}}{T_*^2} \sim 20, \tag{7}$$

(Wyngaard et al., 1971). Thus, if local scaling exists we expect the C_T^2 made dimensionless with local scales to be constant at a magnitude of about 20 in the outer regions of the stable boundary layer as well.

We tested this prediction with numerical data from the Mason and Derbyshire (1990) large-eddy simulation (LES) of the stable boundary layer and with observational data from the 1973 Minnesota experiments (Caughey et al., 1979). The LES domain was 500 m long in the direction of geostrophic wind, 300 m wide, and 1000 m deep. This domain had $40 \times 32 \times 62$ grid points. For analysis of these numerical data we used the Cray-YMP computer facility at the National Center for Atmospheric Research (NCAR). In all cases we used spatial averages over horizontal planes instead of ensemble averages.

We found that over most of the stably stratified layer the dimensionless C_T^2 from the Minnesota measurements is in the range 10–20. The dimensionless C_T^2 from the Mason-Derbyshire LES results is in the range 12–16 over the stable PBL. These show fairly good agreement with the surface-layer asymptote of 20 found in the Kansas data. For the dimensionless C_v^2, the Minnesota data are in the range 10–15 while the LES data yield a value of about 7. The Kansas surface-layer asymptote is about 10, in fairly good

agreement with these other results. Thus, our results support the notion of local scaling of structure-function parameters in the stably stratified boundary layer.

Our results also show that the key governing parameters in local scaling—the temperature flux $\overline{w\theta}(z)$ and shearing stress $\tau(z)$—are very sensitive to unsteadiness of the boundary-layer flow, baroclinity, terrain slope, and breaking gravity waves. As a result, the vertical profiles of $\overline{w\theta}$ and τ are apt to vary strongly from case to case, depending on the magnitudes of these effects. It follows from local scaling that the profiles of C_T^2 and C_v^2 variable as well. The C_T^2 profile is particularly variable; it can either increase or decrease with height, as found experimentally by Cuijpers and Koshiek (1989).

The appendix contains a full report on these results.

2. Structure-function parameters in the convective boundary layer

We also began a study of the structure-function parameters for temperature and humidity in the convective boundary layer. This study was motivated in part by a request from the MIcrowave Remote Sensing Laboratory (MIRSL) at the University of Massachusetts for information on C_N^2 fields in the boundary layer. They need such data for design studies of their Turbulent Eddy Profiler (TEP) radar being developed under a URI grant from ARO.

As an ensemble-average quantity, the structure-function parameter does not fluctuate. In propagation applications, however, it can be necessary to define a "local" structure function parameter which does have a random component. The traditional temperature structure-function parameter is proportional to the inertial-subrange level of the temperature spectrum, and so by the similarity theory for that spectrum can be written (Wyngaard et al., 1971)

$$C_T^2 = 4\beta\epsilon^{-1/3}\epsilon_\theta, \tag{8}$$

Here ϵ and ϵ_θ are the (ensemble-average) molecular destruction rates of turbulent kinetic energy and temperature variance, respectively, and β is the spectral constant. A local temperature structure-function parameter is

$$\tilde{C}_T^2 = 4\beta\tilde{\epsilon}^{-1/3}\tilde{\epsilon}_\theta, \tag{9}$$

where the tilde denotes quantities averaged over a local spatial volume rather than an ensemble of realizations.

With L. Joel Peltier, who is supported by our URI grant from ARO, we are using LES data kindly provided by Chin-Hoh Moeng of NCAR to analyze the behavior of the local structure-function parameter fields for temperature and humidity (defined by averaging over the LES grid volume) in the convective boundary layer. The results show that the vertical profiles of their area averages (which should correspond to the

traditional, ensemble-average parameters) agree well with aircraft data (Wyngaard and LeMone, 1980). However, the local parameters fluctuate considerably; one measure of their variability is the ratio of variance to squared mean,

$$K = \frac{\overline{(\tilde{C}_T^2)^2}}{\overline{(\tilde{C}_T^2)^2}}, \tag{10}$$

where the overbar denotes averaging over the horizontal plane. The LES data indicate that K is of the order of 2–3 in the convective boundary layer. We have begun an extended series of acoustic-sounder-based C_T^2 measurements at our Rock Springs, PA field site, from which we will determine K experimentally.

This work is continuing under our URI grant from ARO.

C. Publications and Presentations

We have no formal publications on this work during the period of the grant, but the appendix is the draft of a manuscript "Similarity of structure-function parameters in the stably stratified boundary layer" that will be submitted for publication shortly.

Dennis Thomson presented an invited paper "Wind-field and turbulence sensing" at the IEEE Topical Symposium on Combined Optical-Microwave Earth and Atmosphere Sensing, 22–25 March, 1993 in Albuquerque. He then traveled to White Sands Missile Range to spend March 26 briefing personnel in the Battlefield Environment Directorate (BED) on current research in boundary-layer meteorology that relates to tactical environmental support systems. A number of opportunities for continuing cooperative research including FM-CW radar and atmospheric acoustical propagation studies were also discussed. Doug Brown of BED organized and hosted Prof. Thomson's visit.

D. Participating Scientific Personnel

Faculty: Dennis Thomson, John Wyngaard.

Graduate students: Robert Edsall, Jeffrey Hare, Branko Kosovic.

E. Bibliography

Caughey, S. J., J. C. Wyngaard, and J. C. Kaimal, 1979: Turbulence in the evolving stable boundary layer. *J. Atmos. Sci.*, **36**, 1041–1052.

Cuijpers, J. W. M., and W. Koshiek, 1989: Vertical profiles of the structure parameter of temperature in the stable, nocturnal boundary layer. *Boundary-Layer Meteorol.*, **47**, 111–129.

Mason, P.J. and S.H. Derbyshire, 1990: Large-eddy simulation of the stably stratified atmospheric boundary layer. *Bound.-Layer Meteor.*, **53**, 117–162.

Nieuwstadt, F.T.M., 1984: Turbulent structure of the stable nocturnal boundary layer. *J. Atmos. Sci.*, **41**, 2202–2216.

Tatarskii, V.I., 1971: The effects of the turbulent atmosphere on wave propagation. Kefer Press, Jerusalem, 472 pp. [NTIS TT 68-50464.]

Wyngaard, J.C., Y. Izumi, and S.A. Collins, Jr., 1971: Behavior of the refractive index structure parameter near the ground. *J. Opt. Soc. Am.*, **61**, 1646–1650.

Wyngaard, J.C., 1973: On surface-layer turbulence. *Workshop on Micrometeorology*, D.A. Haugen, Ed., Amer. Meteor. Soc., Boston, 101–149.

Wyngaard, J. C., W. T. Pennell, D. H. Lenschow, and M. A., LeMone, 1978: The temperature-humidity covariance budget in the convective boundary layer. *J. Atmos. Sci.*, **35**, 47–58.

Wyngaard, J.C. and LeMone, M.A., 1980: Behavior of the refractive index structure parameter in the entraining convective boundary layer. *J. Atmos. Sci.*, **37**, 1573–1585.

APPENDIX

SIMILARITY OF STRUCTURE-FUNCTION PARAMETERS IN THE STABLY STRATIFIED BOUNDARY LAYER

J. Wyngaard and B. Kosovic
Department of Meteorology
Penn State University

Abstract

Published data on the structure-function parameters C_T^2 and C_v^2 of temperature and velocity, respectively, follow Monin-Obukhov (M-O) similarity in the stable surface layer. In the outer layer, C_T^2 and C_v^2 data from the 1973 Minnesota experiments and from the Mason-Derbyshire large-eddy simulation study support Nieuwstadt's local-scaling hypothesis. The data suggest a smooth transition from M-O similarity to local similarity.

The similarity scales in the outer layer depend on the local values of turbulent stress and buoyancy flux, suggesting that remote-sensing measurements of C_T^2 and C_v^2 could be used to infer profiles of stress and buoyancy flux. The local-scaling hypothesis implies, through the mean-flow conservation equations, that the vertical profiles of structure-function parameters are sensitive to unsteadiness, baroclinity, terrain slope, and breaking gravity waves. We show that as a result the C_T^2 profile, in particular, can vary considerably from case to case. This is observed.

1. Introduction

Many boundary-layer researchers will recall the impact of the McAllister et al. (1969) paper. They had pulsed an array of loudspeakers and detected the backscattered energy with the same array. By cleverly recording the signal on a facsimile receiver, they produced striking time-height displays showing how convective eddies rising from the heated surface in the early morning break up the nocturnal boundary layer. Use of the acoustic echo sounder, as it was soon called, spread rapidly; before long, researchers were studying facsimile returns from shallow but distinctly turbulent nocturnal PBLs.

At that time the expected height h of the nocturnal boundary layer was a subject of speculation and controversy (Deardorff, 1972). Similarity theories (e.g., Clarke, 1970) held that h satisfied the equilibrium relation

$$h = \left(\frac{cu_*}{f}\right) F\left(\frac{u_*}{fL}\right), \tag{1}$$

where $c \sim 0.3$, u_* is the friction velocity (the square root of the kinematic surface stress), f is the Coriolis parameter, and L is the Monin-Obukhov length; the function F is unity at neutral and decreases under stable stratification. It was not clear, however, whether the nocturnal boundary layer could reach this equilibrium. The behavior of conventional soundings of temperature and wind had led Blackadar (1957) to conclude that h typically increases during the night from its early-evening minimum. Deardorff suggested that the acoustic echo sounder would be able to provide direct data on $h(t)$ in order to study this question.

Deardorff concluded on the basis of his one-dimensional model calculations that h is generally time dependent and cannot be diagnosed from a steady-state similarity relation such as (1). [He had just carried out time-dependent, fine-mesh, three-dimensional calculations of the neutral and convective PBLs; his attempts to extend these to the stable case failed because most of the turbulence became subgrid-scale. This approach, which we now call large-eddy simulation, or LES, was first applied successfully to the stable case by Mason and Derbyshire (1990).]

Rather than prescribing eddy-diffusivity profiles, as Deardorff had done, Delage (1974) used eddy diffusivities based on predicted turbulent kinetic energy. His one-dimensional model of the nocturnal boundary layer reached a steady state after several hours with a realistic rate of surface cooling. Wyngaard (1975), integrating a full set of second-moment equations, had similar findings.

Brost and Wyngaard (1978) used a simplified form of Wyngaard's second-moment model to calculate the structure and evolution of the stable boundary layer. With a constant surface-cooling rate it could reach an essentially steady state within a few hours. Nieuwstadt (1984) showed that the Brost-Wyngaard equations have steady solutions that display a "local" similarity that is an extension of Monin-Obukhov (M–O) similarity. In M–O similarity the friction velocity u_* and the surface temperature flux $\overline{\theta w}_s$ define the Obukhov length L:

$$L = -\frac{u_*^3}{k(g/T)\overline{\theta w}_s}. \tag{2}$$

Here k is the von Karman constant and g/T is the buoyancy parameter. The counterpart of L in local similarity is the local Obukhov length Λ

$$\Lambda = -\frac{\tau^{3/2}}{k(g/T)\overline{\theta w}}, \tag{3}$$

where $\tau(z)$ is the magnitude of the local kinematic stress (i.e., $\tau^2 = \overline{uw}^2 + \overline{vw}^2$) and $\overline{\theta w}(z)$ is the local temperature flux. Under Nieuwstadt's "local scaling" hypothesis, quantities made dimensionless with τ, $\overline{\theta w}$, and Λ depend only on z/Λ. Nieuwstadt showed that observations taken in the quasi-steady nocturnal PBL at Cabauw, The Netherlands, support this hypothesis.

Nieuwstadt pointed out that while local scaling may be a theoretically satisfactory description of stable turbulence, it is not very well suited for practical applications, which usually require vertical profiles of turbulence; local scaling does not give profiles. However, one can obtain profiles by using local scaling as a closure in model equations for the stable boundary layer. One finds that in general the turbulence profiles depend on the time history of the boundary layer. As Wyngaard (1988) states, "... a simple, diagnostic similarity framework for the *structure* of the nocturnal boundary layer seems not to exist. What we have described instead is a relatively simple model of its *dynamics* .... (Its) solution ... gives the structure, which then depends on the history of the flow and boundary conditions."

2. The Structure-function Parameters

A. Refractive index

Most theoretical analyses of the scattering of electromagnetic, acoustic, and optical radiation by turbulence use the refractive index structure function (Tatarskii, 1971)

which is defined by

$$\overline{[n(\mathbf{x},t) - n(\mathbf{x}+\mathbf{r},t)]^2} \equiv \overline{(n-n')^2}, \tag{4}$$

where n is the fluctuating refractive index at point $\mathbf{x}$ and n' that at point $\mathbf{x}+\mathbf{r}$. The overbar denotes the ensemble average. Many problems of practical importance involve this structure function only for separations $r = |\mathbf{r}|$ in the inertial range of scales, where it has the form

$$\overline{(n-n')^2} = C_N^2 r^{2/3}. \tag{5}$$

Fluctuations in the refractive index for electromagnetic radiation are caused primarily by fluctuations in temperature and absolute humidity, θ and q, respectively. For fluctuation levels typical of the atmospheric boundary layer one can write

$$n = a\theta + bq, \tag{6}$$

where the coefficients a and b depend on the wavelength of the radiation. Wyngaard et al. (1978) have shown that this implies that C_N^2 may be expressed in terms of the structure-function parameters for temperature and humidity, C_T^2 and C_Q^2, and the joint parameter, C_{TQ}:

$$C_N^2 = a^2 C_T^2 + 2abC_{TQ} + b^2 C_Q^2. \tag{7}$$

(For acoustic radiation C_N^2 depends also on the turbulent velocity field.) Functional forms for the coefficients in (7) are summarized by Burk (1979) for acoustic, microwave, and optical radiation. Gossard (1988) has discussed the maintenance of the joint parameter C_{TQ} and its role in radar scattering.

These structure-function parameters are directly proportional to the spectra of temperature and humidity, and their cospectrum, respectively, in the inertial subrange. Similarity arguments due to Kolmogorov, Obukhov, and Corrsin (see Tennekes and Lumley, 1972) indicate that these inertial-range spectral levels depend only on the molecular destruction rates ϵ, χ_θ, χ_q, and $\chi_{\theta q}$ of turbulent kinetic energy, potential temperature and humidity variances, and their covariance, respectively. In the inertial range the one-dimensional spectra behave as (Wyngaard and LeMone, 1980):

$$\begin{aligned}
\Phi_T(\kappa_1) &= 2(2\pi)^{-1}\Gamma(5/3)\sin(\pi/3)C_T^2\kappa_1^{-5/3} \\
&= 0.25C_T^2\kappa_1^{-5/3} = \beta_1\epsilon^{-1/3}\chi_\theta\kappa_1^{-5/3}, \\
Co_{TQ}(\kappa_1) &= 0.25C_{TQ}\kappa_1^{-5/3} = \gamma_1\epsilon^{-1/3}\chi_{\theta q}\kappa_1^{-5/3}, \\
\Phi_Q(\kappa_1) &= 0.25C_Q^2\kappa_1^{-5/3} = \beta_1\epsilon^{-1/3}\chi_q\kappa_1^{-5/3},
\end{aligned} \tag{8}$$

where β_1 and γ_1 are the one-dimensional spectral constants. Our normalization in (8) is such that the integral over the half-line is the covariance. Following Wyngaard and Lemone (1980), we take $\beta_1 = \gamma_1 = 0.4$ and recast (8) as

$$\begin{aligned} C_T^2 &= 1.6\epsilon^{-1/3}\chi_\theta, \\ C_{TQ} &= 1.6\epsilon^{-1/3}\chi_{\theta q}, \\ C_Q^2 &= 1.6\epsilon^{-1/3}\chi_q. \end{aligned} \tag{9}$$

B. Velocity

As discussed by Kaimal (1973), the inertial-subrange form of the velocity structure function for u_1, for example, is

$$\overline{[u_1(\mathbf{x},t) - u_1(\mathbf{x}+\mathbf{r},t)]^2} = C_v^2 r^{2/3}, \tag{10}$$

where C_v^2 is called the velocity structure-function parameter. Kaimal presents the spectral relations analogous to (8). For our purposes we need only the result

$$C_v^2 = 4\alpha_1\epsilon^{2/3} \simeq 2\epsilon^{2/3}, \tag{11}$$

where $\alpha_1 \simeq 0.5$ is the one-dimensional spectral constant for velocity. When acoustic radiation is scattered at angles other than 180 deg, C_v^2 can be the dominant factor in the scattering cross section.

3. Similarity Structure

Eqs. (9) and (11) tie the structure-function parameters to the rates of molecular destruction of the temperature-humidity covariances and of turbulent kinetic energy. We can relate these destruction rates to the dynamics of the turbulence through the second-moment equations. We derive these formally by using the mean-fluctuating decomposition for all random fields (Tennekes and Lumley, 1972). We denote these fields with a tilde, using upper and lower case symbols for their mean and fluctuating parts, respectively:

$$\tilde{u}_i = U_i + u_i; \quad \tilde{p} = P + p; \quad \tilde{T} = \Theta + \theta; \quad \tilde{q} = Q + q. \tag{12}$$

We will use the mixed notation $u_i = (u_1, u_2, u_3) = (u, v, w); x_i = (x_1, x_2, x_3) = (x, y, z)$. Let us assume that conditions are locally homogeneous in the horizontal, so that mean

advection is negligible in the second-moment equations. The potential temperature variance budget is (Wyngaard and Coté, 1971):

$$\frac{\partial\overline{\theta^2}}{\partial t} + 2\overline{\theta w}\frac{\partial\Theta}{\partial z} + \frac{\partial\overline{\theta^2 w}}{\partial z} = -\chi_\theta, \tag{13}$$

The humidity variance and temperature-humidity covariance budgets are (Wyngaard et al., 1978)

$$\frac{\partial\overline{q^2}}{\partial t} + 2\rho\overline{wq}\frac{\partial}{\partial z}\left(\frac{Q}{\rho}\right) + \frac{\partial\overline{q^2 w}}{\partial z} = -\chi_q, \tag{14}$$

$$\frac{\partial\overline{\theta q}}{\partial t} + \overline{wq}\frac{\partial\Theta}{\partial z} + \rho\overline{\theta w}\frac{\partial}{\partial z}\left(\frac{Q}{\rho}\right) + \frac{\partial\overline{\theta q w}}{\partial z} = -\chi_{\theta q}, \tag{15}$$

where ρ is the mean density. Finally, the turbulence kinetic energy (TKE) equation is

$$\frac{\partial}{\partial t}\frac{\overline{u_i u_i}}{2} + \overline{uw}\frac{\partial U}{\partial z} + \overline{vw}\frac{\partial V}{\partial z} + \frac{\partial}{\partial z}\frac{\overline{w u_i u_i}}{2} = \frac{1}{\rho}\frac{\partial\overline{pw}}{\partial z} + \frac{g}{T}\overline{\theta w} - \epsilon, \tag{16}$$

where repeated indices are summed. We are assuming here that the humidity is sufficiently small that it does not contribute significantly to buoyancy; if this is not the case, one can use the same equations but interpret $\tilde{T}$ as the virtual potential temperature (Lumley and Panofsky, 1964).

It seems generally agreed (Panofsky and Dutton, 1984) that to a good approximation in the quasi-steady, locally homogeneous surface layer the budgets of scalar variance and turbulent kinetic energy reduce to a local balance between production and molecular destruction. The $\overline{\theta q}$ budget has not received as much attention, but Wyngaard et al. (1978) found that in the unstable surface layer it does have the same local balance. Since our experience with these second-moment budgets generally indicates that the turbulent transport (i.e., the third-moment divergence) terms are least important under stable conditions, it is plausible that this production-destruction balance for the $\overline{\theta q}$ budget exists under stable conditions as well. Thus, we write (13)–(15) as

$$\chi_\theta = -2\overline{\theta w}\frac{\partial\Theta}{\partial z},$$

$$\chi_q = -2\rho\overline{qw}\frac{\partial}{\partial z}\left(\frac{Q}{\rho}\right),$$

$$\chi_{\theta q} = -\rho\overline{\theta w}\frac{\partial}{\partial z}\left(\frac{Q}{\rho}\right) - \overline{qw}\frac{\partial\Theta}{\partial z}. \tag{17}$$

The TKE equation (16) becomes

$$\epsilon = -\overline{uw}\frac{\partial U}{\partial z} - \overline{vw}\frac{\partial V}{\partial z} + \frac{g}{T_0}\overline{\theta w}. \tag{18}$$

A. Surface-layer similarity

We define surface-layer temperature and humidity scales T_* and q_*,

$$T_* = -\frac{\overline{\theta w}_s}{u_*}, \quad q_* = -\frac{\overline{qw}_s}{u_*}, \tag{19}$$

where $\overline{qw}_s$ is the surface humidity flux. Under the M–O hypothesis in the quasi-steady, locally homogeneous surface layer mean gradients made dimensionless with these scales and height z

$$\phi_h = \frac{kz}{T_*}\frac{\partial \Theta}{\partial z},$$

$$\phi_q = \frac{kz}{q_*}\rho\frac{\partial}{\partial z}\left(\frac{Q}{\rho}\right), \tag{20}$$

are universal functions of z/L. It is not clear whether ϕ_h and ϕ_q differ; we will adopt the suggestion of Panofsky and Dutton (1984) that they be assumed equal. In the surface layer the fluxes of temperature, humidity, and momentum are essentially equal to their surface values, so under the M–O hypothesis we can write (17) as

$$\chi_\theta = \frac{2}{k}\frac{u_* T_*^2}{z}\phi_h; \quad \chi_q = \frac{2}{k}\frac{u_* q_*^2}{z}\phi_h; \quad \chi_{\theta q} = \frac{2}{k}\frac{u_* T_* q_*}{z}\phi_h. \tag{21}$$

We choose the x-axis along the mean wind, so that $U_i = [U(z), 0, 0]$ and the M–O function for mean wind shear is

$$\phi_m = \frac{kz}{u_*}\frac{\partial U}{\partial z}. \tag{22}$$

We can write the dissipation-rate expression (18) as

$$\epsilon = \frac{u_*^3}{kz}\left(\phi_m - z/L\right). \tag{23}$$

Combining (9), (21), and (23) then yields M–O expressions for the refractive index structure-function parameters:

$$C_T^2 = \frac{3.2}{k^{2/3}}\frac{T_*^2}{z^{2/3}}\phi_h\left(\phi_m - z/L\right)^{-1/3},$$

$$C_Q^2 = \frac{3.2}{k^{2/3}} \frac{q_*^2}{z^{2/3}} \phi_h (\phi_m - z/L)^{-1/3},$$

$$C_{TQ} = \frac{3.2}{k^{2/3}} \frac{q_* T_*}{z^{2/3}} \phi_h (\phi_m - z/L)^{-1/3}. \tag{24}$$

That for velocity is

$$C_v^2 = \frac{2}{k^{2/3}} \frac{u_*^2}{z^{2/3}} (\phi_m - z/L)^{2/3}. \tag{25}$$

There are two important aspects of the expressions in (24). First, they predict that the structure-function parameters made dimensionless with the surface-layer scales vary identically with the stability parameter z/L. Second, the structure parameter C_{TQ} is not positive definite, as are the other two; its sign is that of $T_* q_*$—i.e., that of the product of the surface fluxes of temperature and humidity. Under stably stratified conditions the surface temperature flux is negative; we would normally expect the surface humidity flux to be positive, making C_{TQ} negative.

Of the three refractive-index structure-function parameters only C_T^2 has been measured extensively. The Kansas results (Businger et al., 1971) indicate for stable conditions

$$\phi_h = 0.74 + 4.7 z/L; \quad \phi_m = 1.0 + 4.7 z/L, \tag{26}$$

so that with the Kansas value of 0.35 for k the M–O form (24) for C_T^2 becomes

$$\frac{C_T^2 z^{2/3}}{T_*^2} = \frac{4.8(1 + 6.35 z/L)}{(1 + 3.7 z/L)^{1/3}}, \tag{27}$$

Figure 1 shows C_T^2 data from the 1968 Kansas experiments (Wyngaard et al., 1971), the 1973 Minnesota experiments (Caughey et al., 1979), and from experiments reported by Foken and Kretschmer (1990). Eq. (27) fits those results fairly well.

B. The stable surface-layer asymptote

Under very stable conditions (large z/L) our expression (27) for C_T^2 becomes

$$\frac{C_T^2 z^{2/3}}{T_*^2} \simeq 20 (z/L)^{2/3}. \tag{28}$$

Eq. (25) for C_v^2 becomes, using (26),

$$\frac{C_v^2 z^{2/3}}{u_*^2} \simeq 9.6 (z/L)^{2/3}. \tag{29}$$

These can be rewritten as

$$C_T^2 \simeq 20\frac{T_*^2}{L^{2/3}}, \qquad C_v^2 \simeq 9.6\frac{u_*^2}{L^{2/3}}. \tag{30}$$

A "local $z-$less stratification" interpretation of (30) (Wyngaard, 1973) is that under very stable conditions turbulent eddy sizes are restricted by stability and z loses significance as a length scale for the turbulence. Then the only length scale L, the only temperature scale is T_*, and the only velocity scale is u_*, so that C_T^2 and C_v^2 must scale with $T_*^2/L^{2/3}$ and $u_*^2/L^{2/3}$, respectively. Both the flux and gradient Richardson numbers approach constants interpreted as their limiting values for stable stratification.

C. Outer-layer similarity

Let us briefly review the physics underlying the notion of local scaling of turbulence in the stably stratified boundary layer and the evidence supporting it.

Progress in turbulence has traditionally been paced by observational studies (Bradshaw, 1972). Because observations are usually more difficult and expensive in geophysical flows than in the laboratory, our understanding of the atmospheric boundary layer has lagged that of engineering boundary layers. When the requisite micrometeorological turbulence sensors and data-acquisition systems became available by the 1960s, researchers studied in detail the turbulence structure of the surface layer and the transport processes within it. The 1968 Kansas experiments (Haugen et al., 1971), for example, documented this structure over a wide range of stability conditions. Such experiments at ideal sites showed that under stable conditions the second-moment budgets displayed a characteristic state of local equilibrium in which the time-change and turbulent transport (third-moment flux divergence) terms were small and the production and destruction rates were in balance, as exhibited in Eqs. (17) and (18). Furthermore, the data behaved as if L rather than z determines the length scale of the turbulence. These findings stood in striking contast with those for the unstable surface layer.

Numerical models of the stably stratified boundary layer, using closures rooted in this interpretation of the surface-layer physics, gradually appeared (Delage, 1974; Brost and Wyngaard, 1978; Nieuwstadt, 1984). They might have seemed bold extrapolations, but there were indications that they could account fairly well for behavior observed in at least some experiments (Caughey et al., 1979; Nieuwstadt, 1984). However, others showed features such as flow intermittency under very stable conditions (Kondo et al., 1978) and gravity-wave effects (de Baas and Driedonks, 1985) that were not accounted for or reproduced by numerical models.

When the stably stratified boundary layer yielded to large-eddy simulation (Mason and Derbyshire, 1990), a new avenue to studying its structure and dynamics was opened. Derbyshire (1990) soon suggested that a key parameter is $B_0/G^2 f$, where B_0 is the surface buoyancy flux and G is the magnitude of the geostrophic wind. He argued that when this parameter is less than a threshold value the layer can exist in a quasi-steady state. Mason and Derbyshire stated that "The potentially nonlocal character of some wave motions does not seem to be strong enough to invalidate local scaling .... Arguments given by Derbyshire (1990) show that this is to be expected if the waves are generated purely by turbulence, though topographic waves may of course behave differently." In the quasi-steady state and without topography, the Mason-Derbyshire results indicate broad agreement with the local-scaling hypothesis for the nocturnal boundary layer.

Under the local scaling hypothesis we can write for the outer layer

$$C_T^2 = \frac{(\overline{\theta w})^2}{\tau \Lambda^{2/3}}\, f_1(z/\Lambda), \quad C_v^2 = \frac{\tau}{\Lambda^{2/3}}\, f_2(z/\Lambda). \tag{31}$$

where f_1 and f_2 are functions to be determined. The vanishing significance of z under strong stratification implies that they approach constants in the limit $z/\Lambda \to \infty$. The flux and gradient Richardson numbers are also constant at their limiting values. The Brost-Wyngaard model gives in this stable limit

$$f_1 = \frac{6.2\widetilde{\overline{w^2}}^{1/6}}{\widetilde{K}_h^{5/6}\tilde{q}}, \quad f_2 = \frac{0.54\tilde{q}^2}{\widetilde{\overline{w^2}}^{1/3}\widetilde{K}_h^{1/3}}, \tag{32}$$

where K_h is the eddy diffusivity for temperature, q^2 is twice the turbulent kinetic energy per unit mass, and a tilde denotes nondimensionalization with the local scales $\overline{\theta w}, \tau$, and Λ. Each of these dimensionless dependent variables is a function of z/Λ. Nieuwstadt's numerical solutions show that as z/Λ increases they approach constant values of

$$\widetilde{K}_h \simeq 0.08, \quad \tilde{q} \simeq 2.9, \quad \widetilde{\overline{w^2}} \simeq 1.7, \tag{33}$$

so that from (32)

$$f_1 \simeq 19, \quad f_2 \simeq 9, \tag{34}$$

and

$$C_T^2 \simeq 19\frac{(\overline{w\theta})^2}{\tau \Lambda^{2/3}}, \quad C_v^2 \simeq 9\frac{\tau}{\Lambda^{2/3}}. \tag{35}$$

These agree well with the surface-layer asymptotes in Eq. (30), because the closure constants in the Brost-Wyngaard model were chosen so that its results were compatible with the stable limit. This is consistent with Sorbjan's (1986) hypothesis that for a given variable the forms of the M–O and outer-layer similarity functions are the same.

We tested the predictions (35) of the local-scaling hypothesis with LES results and with experimental data. The results from the Mason-Derbyshire (1990) LES study of the stably stratified boundary layer indicate that C_T^2 made dimensionless with local scales approaches an asymptote of about 12 (Figure 2), and that C_v^2 so nondimensionalized has an asymptote of about 7 (Figure 3). These asymptotes agree fairly well with those of (35).

The experimental data were taken at $0.3 < z/h < 0.75$ in the 1973 Minnesota experiment (Caughey et al., 1979). Unfortunately only $\overline{uw}$ data are available; the lateral stress $\overline{vw}$ was contaminated by balloon motion. Thus, in calculating the local scaling parameter τ we neglected the contribution of $\overline{vw}$, which is difficult to justify near h. The Minnesota C_T^2 and C_v^2 data so scaled are plotted in Figures 4 and 5, respectively. In general they agree well with the local-scaling results (35) and the Mason-Derbyshire LES results.

4. Vertical Profiles

From (30) and (35) we can write for most of the stable boundary layer—from the outer edge of the surface layer through the outer layer—

$$C_T^2(z) \simeq 20 \left(k\frac{g}{T}\right)^{2/3} \frac{|\overline{\theta w}|^{8/3}}{\tau^2}, \quad C_v^2(z) \simeq 9 \left(k\frac{g}{T}\right)^{2/3} |\overline{\theta w}|^{2/3}. \tag{36}$$

Eq. (36) shows that the C_T^2 profile depends on the profiles of kinematic stress magnitude $\tau(z)$ and temperature flux $\overline{\theta w}(z)$; we will see that the balance here is so delicate that C_T^2 can either increase or decrease with height. By contrast, the profile of C_v^2 depends only on the $\overline{\theta w}$ profile, so that we expect it to decrease monotonically with height. Let us now consider the behavior of the τ and $\overline{\theta w}$ profiles in more detail.

A. Steady conditions

In the simplest steady case with horizontal homogeneity and z-independent geostrophic wind components U_g and V_g, the equations for the vertical gradients of mean

wind and temperature reduce to

$$\frac{\partial^2 \overline{uw}}{\partial z^2} = f\frac{\partial V}{\partial z}, \quad \frac{\partial^2 \overline{vw}}{\partial z^2} = -f\frac{\partial U}{\partial z}, \tag{37}$$

$$\frac{\partial^2}{\partial z^2}\overline{\theta w} = 0. \tag{38}$$

Using the boundary conditions that $\overline{w\theta} = \overline{\theta w}_s$ at $z = 0$ and $\overline{\theta w} = 0$ at $z = h$, (38) yields the steady-state $\overline{\theta w}$ profile

$$\overline{\theta w} = \overline{\theta w}_s(1 - z/h). \tag{39}$$

Nieuwstadt (1984) showed also that a stress closure based on local scaling gives a solution of (37) whose τ profile is

$$\tau = u_*^2(1 - z/h)^{3/2}. \tag{40}$$

It follows from (36) that the steady profiles of C_T^2 and C_v^2 from the outer edge of the surface layer through the outer layer are

$$C_T^2 \simeq 20\frac{T_*^2}{L^{2/3}}(1 - z/h)^{-1/3}, \quad C_v^2 \simeq 9\frac{u_*^2}{L^{2/3}}(1 - z/h)^{2/3}. \tag{41}$$

Eq. (41) predicts that C_T^2 increases with height, but the observations of Caughey et al. (1979) and Cuijpers and Koshiek (1989) show that it decreases. The prediction of an increasing C_T^2 profile results from the steady-state balance between the competing effects of $\overline{\theta w}$, which causes C_T^2 to decrease with height, and τ, which causes it to increase. Let us now examine other factors that can influence the shapes of the $\overline{\theta w}$ and τ profiles and, hence, change this balance.

B. Influences on the structure-parameter profiles

The stress and temperature-flux profiles are coupled to the mean horizontal momentum and mean potential temperature equations, respectively. Let us consider several influences on those equations and therefore on the vertical profile of C_T^2.

1. Time changes

During its early phases, at least, the nocturnal PBL must be unsteady. Near sundown the changing surface energy balance causes the surface heat flux to change from positive to negative; in a horizontally homogeneous case the mean potential temperature gradient in the air above must then evolve according to

$$\frac{\partial}{\partial t}\frac{\partial \Theta}{\partial z} + \frac{\partial^2 \overline{\theta w}}{\partial z^2} = 0. \tag{42}$$

In the initial stages of evolution $\partial\Theta/\partial z$ grows in time, so that $\partial^2\overline{\theta w}/\partial z^2$ is negative. Let us now estimate the departures from a linear $\overline{\theta w}$ profile this causes.

For illustrative purposes let the $\overline{\theta w}$ profile in the evolving nocturnal PBL be

$$\overline{\theta w} = Q_0(1 - z/h) + 4\delta\overline{\theta w}\frac{z}{h}\left(1 - \frac{z}{h}\right), \tag{43}$$

where $\delta\overline{\theta w}$ is the midlayer departure from the linear profile in steady state. We scale the terms in the mean temperature evolution equation as

$$\frac{\partial^2\overline{\theta w}}{\partial z^2} = -\frac{8\delta\overline{\theta w}}{h^2}, \quad \frac{\partial}{\partial t}\frac{\partial\Theta}{\partial z} \sim \frac{1}{\tau_t}\frac{\Delta\Theta}{h}, \tag{44}$$

where Δ denotes the change across the boundary layer and τ_t is a time scale. Thus, the balance is

$$\frac{\delta\overline{\theta w}}{Q_0} \sim \frac{h\Delta\Theta}{8\tau Q_0}. \tag{45}$$

For typical values $h = 200$ m, $\Delta\Theta = 5$ K, $\tau_t = 12$ h, and $\overline{\theta w}_s = -0.01$ m K s^{-1}, (45) yields $\delta\overline{\theta w}/\overline{\theta w}_s \simeq -1/4$. Then to a good approximation the $\overline{\theta w}$ profile (43) becomes in this case

$$\overline{\theta w} \simeq \overline{\theta w}_s(1 - z/h) - \overline{\theta w}_s\frac{z}{h}\left(1 - \frac{z}{h}\right) = \overline{\theta w}_s(1 - z/h)^2. \tag{46}$$

The data on $\overline{\theta w}$ from the rapidly evolving, early evening boundary layers in the Minnesota experiment (Caughey et al., 1979) are fit well by (46).

The departure from linearity of $\overline{\theta w}$ caused by time changes has a strong effect on the C_T^2 profile. Eq. (36) shows that a linear $\overline{\theta w}$ profile gives C_T^2 increasing as $(1 - z/h)^{-1/3}$, while a parabolic $\overline{\theta w}$ profile yields C_T^2 decreasing as $(1 - z/h)^{7/3}$.

Under unsteady but horizontally homogeneous conditions the z-derivatives of mean horizontal momentum equations are

$$\frac{\partial^2\overline{uw}}{\partial z^2} = f\frac{\partial V}{\partial z} - \frac{\partial}{\partial t}\frac{\partial U}{\partial z}, \quad \frac{\partial^2\overline{vw}}{\partial z^2} = -f\frac{\partial U}{\partial z} - \frac{\partial}{\partial t}\frac{\partial V}{\partial z}. \tag{47}$$

These show that time changes modify the existing curvature of the stress profiles.

2. Baroclinity

Let the flow be steady and horizontally homogeneous except for mean temperature gradients in x and y. The vertical gradients of U_g and V_g are given hydrostatically by

$$\frac{\partial U_g}{\partial z} = -\frac{g}{fT}\frac{\partial T}{\partial y}, \quad \frac{\partial V_g}{\partial z} = \frac{g}{fT}\frac{\partial T}{\partial x}. \tag{48}$$

The mean-gradient equations are now

$$\frac{\partial^2 \overline{uw}}{\partial z^2} = f\left(\frac{\partial V}{\partial z} - \frac{\partial V_g}{\partial z}\right), \quad \frac{\partial^2 \overline{vw}}{\partial z^2} = f\left(\frac{\partial U_g}{\partial z} - \frac{\partial U}{\partial z}\right), \tag{49}$$

$$\frac{\partial^2 \overline{w\theta}}{\partial z^2} = \frac{fT}{g}\left(\frac{\partial V}{\partial z}\frac{\partial U_g}{\partial z} - \frac{\partial U}{\partial z}\frac{\partial V_g}{\partial z}\right), \tag{50}$$

showing that baroclinity can also induce curvature in the flux profiles. From (49) the effect on the stress profiles will be significant if the geostrophic wind shear is an appreciable fraction of the wind shear. From (48) we see that in midlatitudes a horizontal temperature gradient of 3 K per 100 km, not an unusually large value, causes a geostrophic wind shear of 10 m s^{-1} per kilometer. This is comparable to the wind shear, so we conclude that typical magnitudes of baroclinity do have a substantial effect on the stress profile.

Let us use (50) to estimate the geostrophic wind shear required to generate significant departure of the $\overline{\theta w}$ profile from linearity. Denoting the magnitude of the mean wind as S, we scale the terms in (50) as:

$$\frac{8\delta\overline{w\theta}}{h^2} \sim \frac{fT}{g}\frac{\Delta S}{h}\frac{\Delta G}{h}. \tag{51}$$

Writing (51) as an expression for the fractional change in midlayer temperature flux, we find

$$\frac{2\delta\overline{w\theta}}{\overline{\theta w}_s} = \frac{fT}{4g}\frac{\Delta S \Delta G}{\overline{\theta w}_s}. \tag{52}$$

For midlatitudes, $\overline{\theta w}_s = -0.01$ m s^{-1} K, and $\Delta S \Delta G = 10$ m^2 s^{-2}, (52) gives a 70% change in the midlayer temperature flux.

3. Terrain slope

Consider a nocturnal PBL that is homogeneous in planes parallel to a land surface that slopes at an angle β to the horizontal. Then the steady mean wind gradient equations in coordinates aligned with the sloping terrain are (Brost and Wyngaard, 1978)

$$\frac{\partial^2 \overline{uw}}{\partial z^2} = f\frac{\partial V}{\partial z} - \frac{g}{T}\frac{\partial \Theta}{\partial z}|\beta|\cos\gamma, \quad \frac{\partial^2 \overline{vw}}{\partial z^2} = -f\frac{\partial U}{\partial z} + \frac{g}{T}\frac{\partial \Theta}{\partial z}|\beta|\sin\gamma. \tag{53}$$

Here γ is the angle, measured counterclockwise, from the fall-line vector (the vector perpendicular to the contour lines and pointing down the slope) to the x-axis. Let us use

(53) to estimate the threshold terrain slope that gives a drainage term that appreciably changes the stress profile. We do this simply by equating the magnitudes of the drainage and Coriolis terms. This yields

$$\beta \sim \frac{f\Delta ST}{g\Delta\Theta}. \tag{54}$$

For $\Delta S = 10$ m s^{-1} and $\Delta\Theta = 5$ K this gives $\beta \sim 1.5 \times 10^{-3}$, a terrain slope of 1.5 parts per thousand. This is the slope of the unusually flat Minnesota site (Caughey et al., 1979). We conclude that terrain-slope effects on the stress profile are apt to be significant.

4. Internal gravity waves

De Baas and Driedonks (1985) observed nocturnal PBL structure from the 200-m tower at Cabauw, The Netherlands. On occasion they detected Kelvin-Helmholtz waves with frequencies in the range 3×10^{-3} Hz to 2×10^{-2} Hz that persisted as quasi-steady oscillations for as long as one hour without breaking into turbulence. Their presence was seen not only in the time series of fluctuations, but also in the increase of the vertical velocity and temperature variances with height.

Einaudi and Finnigan (1981) analyzed a nearly monochromatic wave of 240 s period detected in a weakly stable, nocturnal boundary layer at the Boulder Atmospheric Observatory. They found that linear wave theory described the wave properties and the vertical structure of the w and θ fluctuations well. In a second paper (Finnigan and Einaudi, 1981) they showed that while the wave-like fluctuations in Reynolds stress were larger than the background turbulent stress levels, they were nearly in quadrature with the gradients of wave velocity, so they did not extract energy from the wave at an appreciable rate; as a result, the wave could persist in a quasi-steady state. They found that the turbulence time scale was longer than the wave period, however, so the turbulence was not in equilibrium with the large, wave-frequency fluctuations in shear production.

Coulter (1990) found that the turbulence levels in the nocturnal PBL over gently rolling terrain in northeastern Illinois were quite different on consecutive nights with similar mean conditions. Turbulence levels were low on the first night, but during the second night the signals showed evidence of waves of two-minute period that grew and extended beyond the PBL depth at approximately 60-minute intervals. The records showed clearly defined active and inactive periods, with the differences in turbulence parameters σ_w, N, and ϵ ranging from a factor of 2 to 4 between them. Coulter interpreted the two-minute periodicities as Kelvin-Helmholtz waves made detectable to the

acoustic sounder through their modulation of the local turbulence structure. He inferred that they grew rapidly in amplitude with time until they overturned and broke into turbulence; that destroyed the wind shear and temperature gradient temporarily, but within about 30 minutes the cycle was renewed.

These studies indicate that the nocturnal PBL can have strong gravity-wave activity that modifies its turbulence structure. In view of the Finnigan-Einaudi finding that the time scales of the wave and the turbulence can be of the same order, we must conclude that the local-scaling relations for structure-function parameters could be modified as well. For this reason, in his analysis Nieuwstadt (1984) excluded cases with strong gravity waves by including only those for which $\overline{w^2}$ decreased continuously with height. He then used a high-pass filter on the time series, as did Caughey et al. (1979).

C. Implications for remote sensing

We have shown that the sensitivity of structure-parameter profiles in the stable PBL to typical magnitudes of flow unsteadiness, baroclinity, and terrain slope precludes their universality in the typical nocturnal PBL. This is consistent with the findings of Cuijpers and Koshiek (1988). Their measured C_T^2 profiles in the nocturnal boundary layer were not fit well by the steady state models of Nieuwstadt (1984, 1985) or Sorbjan (1986). The numerical model of Duynkerke and Driedonks (1987), which uses closures similar to those of Nieuwstadt but allows for time evolution of the boundary layer, gave the best results.

Nonetheless, the similarity expressions (36) that relate local values of the structure parameters to local turbulence parameters are consistent with observations, LES results, and model predictions. This has interesting implications for remote sensing. From the second of (36) we see that a measurement of C_v^2 yields the temperature flux directly:

$$\overline{\theta w} = -\frac{0.037T}{kg}\left(C_v^2\right)^{3/2}. \tag{55}$$

A measurement of C_T^2 as well then yields the stress magnitude from the first of (36):

$$\tau = \frac{0.055T}{kg}\frac{\left(C_v^2\right)^2}{\left(C_T^2\right)^{1/2}}. \tag{56}$$

Neff and Coulter (1986) and Gossard (1992) have discussed the measurement of structure-parameter profiles with ground-based remote sensors.

If the measured C_T^2 and C_v^2 have errors $\epsilon(C_T^2)$ and $\epsilon(C_v^2)$, then from (55) and (56) the errors in the inferred fluxes are, to first order,

$$\frac{\epsilon(\overline{w\theta})}{\overline{w\theta}} = \frac{3}{2}\frac{\epsilon(C_v^2)}{C_v^2}, \quad \frac{\epsilon(\tau)}{\tau} = 2\frac{\epsilon(C_v^2)}{C_v^2} - \frac{1}{2}\frac{\epsilon(C_T^2)}{C_T^2}, \tag{57}$$

showing that the technique is considerably more sensitive to errors in C_v^2 than in C_T^2.

5. Conclusions

The local-scaling hypothesis holds that over most of the nocturnal boundary layer the turbulence is near its critical Ricardson number and its length, velocity, and temperature scales are determined by the local stress and buoyancy flux. Data from several field experiments and the Mason-Derbyshire large-eddy simulation study show that the structure-function parameters for temperature and velocity are consistent with local scaling. The vertical profiles of the structure-function parameters are apt to be highly variable because of the sensitivity of the stress and temperature flux profiles to unsteadiness of the flow, baroclinity, and terrain slope. The local scaling result does offer the prospect that the stress and temperature flux profiles can be inferred from measurements of the structure-function parameter profiles, however.

Acknowledgments

The authors are grateful to Drs. P. J. Mason and S. H. Derbyshire for providing us with their LES data and to Drs. E. Andreas, D. Thomson, and J. Peltier for helpful discussions. This work was supported by the U. S. Army Research Office.

Figure Captions

1. Experimental data on C_T^2 in the stable surface layer, presented in M–O coordinates.

2. C_T^2 data from the Mason-Derbyshire large-eddy simulation study of the nocturnal boundary layer, presented in local-scaling coordinates.

3. C_v^2 data from the Mason-Derbyshire large-eddy simulation study of the nocturnal boundary layer, presented in local-scaling coordinates.

4. A test of the local-scaling prediction that the dimensionless C_T^2 approaches a constant. The Minnesota data are averages over a few measurements; the symbol represents the mean and the bracket indicates plus and minus one standard error.

5. A test of the local-scaling prediction that the dimensionless C_v^2 approaches a constant.

References

Blackadar, A. K., 1957: Boundary-layer wind maxima and their significance for the growth of nocturnal inversions. *Bull. Amer. Meteorol. Soc.*, **38**, 283–290.

Bradshaw, P., 1972: The understanding and prediction of turbulent flow. *Aeronaut. J.*, **76**, 403–418.

Brost, R. A., and J. C. Wyngaard, 1978: A model study of the stably stratified planetary boundary layer. *J. Atmos. Sci.*, **35**, 1427–1440.

Burk, S. D., 1979: Refractive index structure parameters: Time-dependent calculations using a numerical boundary-layer model. *J. Appl. Meteorol.*, **19**, 562–576.

Businger, J. A., J. C. Wyngaard, Y. Izumi and E. F. Bradley, 1971: Flux-profile relationships in the atmospheric surface layer. *J. Atmos. Sci.*, **28**, 181–189.

Caughey, S. J., J. C. Wyngaard, and J. C. Kaimal, 1979: Turbulence in the evolving stable boundary layer. *J. Atmos. Sci.*, **36**, 1041–1052.

Clarke, R. H., 1970: Observational studies in the atmospheric boundary layer. *Quart. J. Roy. Meteorol. Soc.*, **96**, 91–114.

Coulter, R. L., 1990: A case study of turbulence in the stable nocturnal boundary layer. *Boundary-Layer Meteorol.*, **52**, 75–91.

Cuijpers, J. W. M., and W. Koshiek, 1989: Vertical profiles of the structure parameter of temperature in the stable, nocturnal boundary layer. *Boundary-Layer Meteorol.*, **47**, 111–129.

Deardorff, J. W., 1972: Rate of growth of the nocturnal boundary layer. *Proceedings of the Symposium on Air Pollution, Turbulence and Diffusion, December, 1971*, H. W. Church and R. E. Luna, Eds., Sandia Laboratories, Albuquerque, NM.

de Baas, A. F., and A. G. M. Driedonks, 1985: Internal gravity waves in a stably stratified boundary layer. *Boundary-Layer Meteor.*, **31**, 303–323.

Delage, Y., 1974: A numerical study of the nocturnal atmospheric boundary layer. *Quart. J. Roy. Meteorol. Soc.*, **100**, 351–364.

Derbyshire, S. H., 1990: Nieuwstadt's stable boundary layer revisited. *Quart. J. Roy. Meteor. Soc.*, **116**, 127–158.

Einaudi, F., and J. J. Finnigan, 1981: The interaction between an internal gravity

wave and the planetary boundary layer. Part I: The linear analysis. *Quart. J. Roy. Meteorol. Soc.*, **107**, 793–806.

Finnigan, J. J. and F. Einaudi, 1981: The interaction between an internal gravity wave and the planetary boundary layer. Part II: Effect of the wave on the turbulence structure. *Quart. J. Roy. Meteorol. Soc.*, **107**, 807–832.

Foken, T., and D. Kretschmer, 1990: Stability dependence of the temperature structure parameter. *Boundary-Layer Meteorol.*, **53**, 185–189.

Gossard, E. E., 1988: Measuring gradients of meteorological properties in elevated layers with a surface-based Doppler radar. *Radio Science*, **23**, 625–639.

Gossard, E. E., 1992: Relationship of height gradients of passive atmospheric properties to their variances: Applications to the ground-based remote sensing of profiles. NOAA Technical Report ERL 448-WPL 64. Available from NTIS.

Haugen, D. A., J. C. Kaimal, and E. F. Bradley, 1971: An experimental study of Reynolds stress and heat flux in the atmospheric surface layer. *Quart. J. Roy. Meteor. Soc.*, **97**, 168–180.

Kaimal, J. C., 1973: Turbulence spectra, length scales and structure parameters in the stable surface layer. *Boundary-Layer Meteorol.*, **4**, 289–309.

Kondo, J., O. Kanechika, and N. Yasuda, 1978: Heat and momentum transfers under strong stability in the atmospheric surface layer. *J. Atmos. Sci.*, **35**, 1012–1021.

Lumley, J. L., and H. A. Panofsky, 1964: *The Structure of Atmospheric Turbulence.* Interscience, New York, 239 pp.

Mason, P. J., and S. H. Derbyshire, 1990: Large-eddy simulation of the stably stratified atmospheric boundary layer. *Boundary-Layer Meteorol.*, **53**, 117–162.

McAllister, L. G., J. R. Pollard, A. R. Mahoney, and P. J. R. Shaw, 1969: Acoustic sounding—A new approach to the study of atmospheric structure. *Proc. IEEE*, **57**, 579–587.

Neff, W. D., and R. L. Coulter, 1986: Acoustic remote sensing. *Probing the Atmospheric Boundary Layer*, D. H. Lenschow, Ed., Amer. Meteorol. Soc., Boston, 201–239.

Nieuwstadt, F. T. M., 1984: The turbulent structure of the stable, nocturnal boundary layer. *J. Atmos. Sci.*, **41**, 2202–2216.

Nieuwstadt, F. T. M., 1985: A model for the stationary, stable boundary layer. *Turbulence and Diffusion in Stable Environments*, J. C. R. Hunt, Ed., Clarendon Press, Oxford, 149–179.

Panofsky, H. A., and J. A. Dutton, 1984: *Atmospheric Turbulence.* Wiley, New York, 397 pp.

Sorbjan, Z., 1986: On similarity in the atmospheric boundary layer. *Boundary-Layer Meteorol.*, **34**, 2430–2432.

Tatarskii, V. I., 1971: *The Effects of the Turbulent Atmosphere on Wave Propagation.* Kefer Press, Jerusalem, 472 pp. [NTIS TT 68-50464].

Tennekes, H., and J. L. Lumley, 1972: *A First Course in Turbulence.* MIT Press, Cambridge, 300 pp.

Wyngaard, J. C., 1973: On surface-layer turbulence. *Workshop on Micrometeorology*, D. A. Haugen, Ed., Amer. Meteorol. Soc., Boston, 392 pp.

Wyngaard, J. C., 1975: Modeling the planetary boundary layer—Extension to the stable case. *Boundary-Layer Meteorol.*, **9**, 441–460.

Wyngaard, J. C., 1988: Structure of the PBL. *Lectures on Air Pollution Modeling*, A. Venkatram and J. Wyngaard, Eds., Amer. Meteorol. Soc., Boston, 390 pp.

Wyngaard, J. C., and O. R. Coté, 1971: The budgets of turbulent kinetic energy and temperature variance in the atmospheric surface layer. *J. Atmos. Sci.*, **28**, 190–201.

Wyngaard, J. C., Y. Izumi, and S. A. Collins, Jr., 1971: Behavior of the refractive index structure parameter near the ground. *J. Opt. Soc. Amer.*, **61**, 1646–1650.

Wyngaard, J. C., W. T. Pennell, D. H. Lenschow, and M. A., LeMone, 1978: The temperature-humidity covariance budget in the convective boundary layer. *J. Atmos. Sci.*, **35**, 47–58.

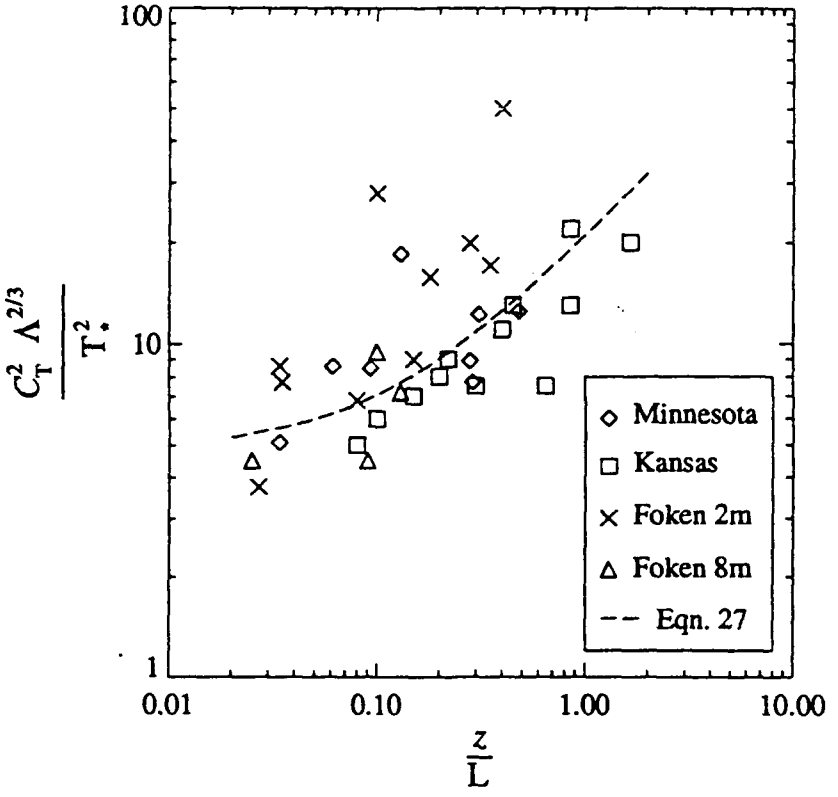
100
10
1
0.01
0.10
1.00
10.00
$\frac{C_T^2 \Lambda^{2/3}}{T_*^2}$
$\frac{z}{L}$
Minnesota
Kansas
Foken 2m
Foken 8m
Eqn. 27

Figure 1

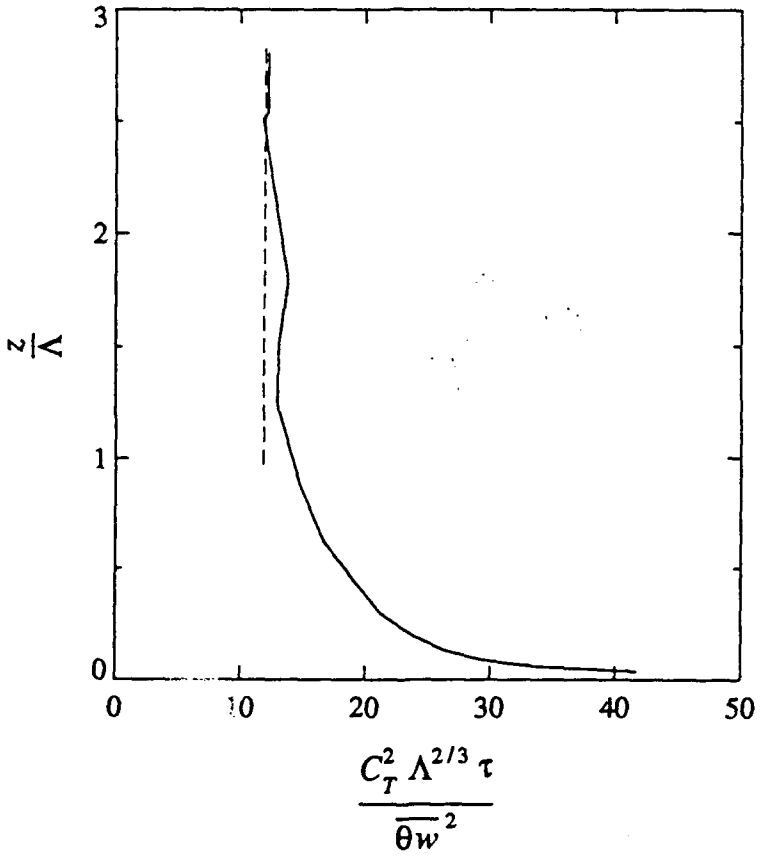
3
2
1
0
0
10
20
30
40
50
z/Λ
$\frac{C_T^2 \Lambda^{2/3} \tau}{\overline{\theta w}^2}$

Figure 2

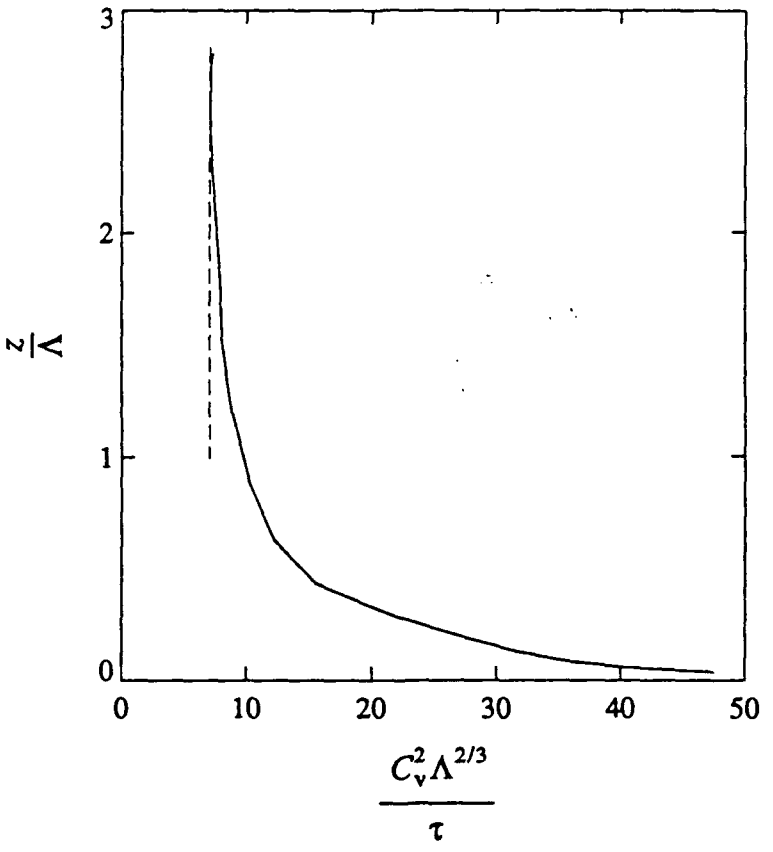

Figure 3

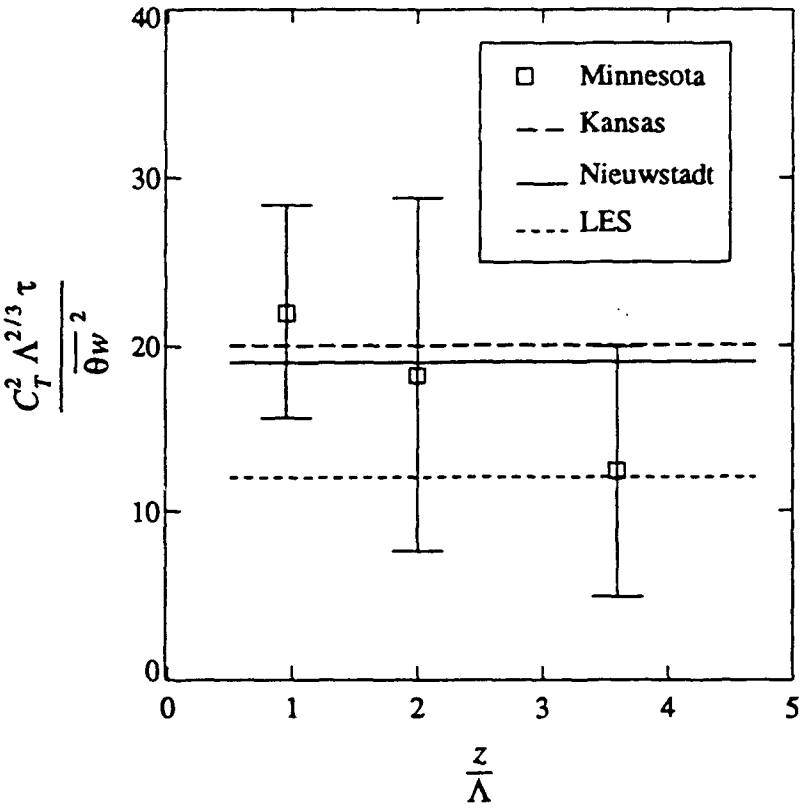
Minnesota
Kansas
Nieuwstadt
LES
40
30
20
10
0
0
1
2
3
4
5
$\frac{C_T^2 \Lambda^{2/3} \tau}{\overline{\theta w}^2}$
$\frac{z}{\Lambda}$

Figure 4

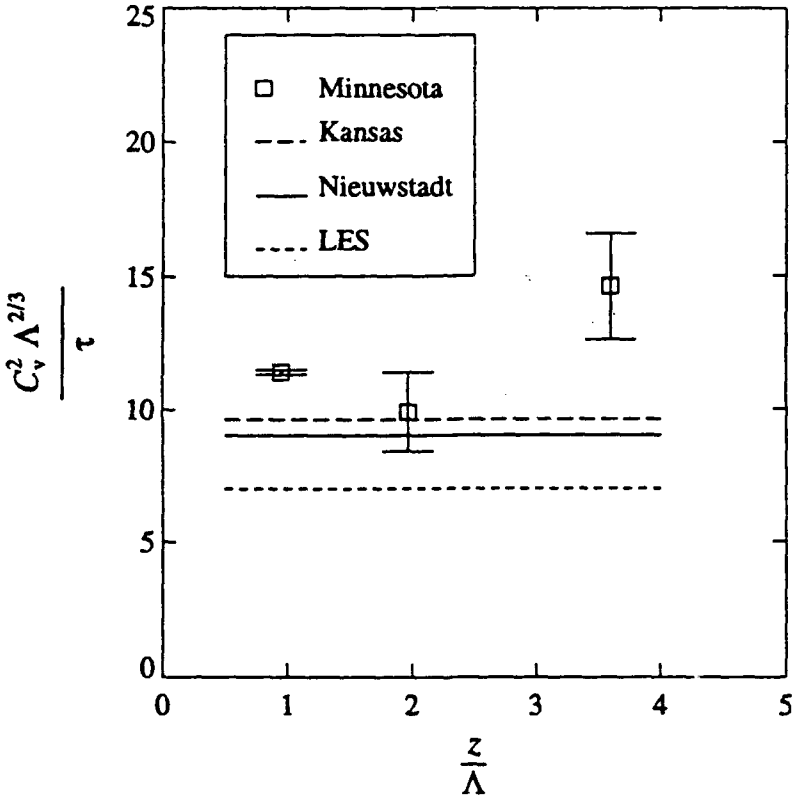
Minnesota
Kansas
Nieuwstadt
LES
$\frac{C_v^2 \Lambda^{2/3}}{\tau}$
$\frac{z}{\Lambda}$
0
5
10
15
20
25
0
1
2
3
4
5

Figure 5